JOURNAL OF MATERIALS SCIENCE 30 (1995) 1912–1920

Modification of Hypoeutectic Al–Si alloys

C. R. HO, B. CANTOR,
Oxford Centre for Advanced Materials and Composites, Department of Materials, University of Oxford, Parks Road, Oxford OX1 3PH, UK

Modification of the Al–Si eutectic microstructure has been studied by using the entrained droplet technique in a range of hypoeutectic Al–Si alloys doped with different levels of phosphorus and sodium. Differential scanning calorimetry has been used to investigate the kinetics of silicon nucleation during eutectic solidification, and transmission and scanning transmission electron microscopy has been used to investigate the eutectic microstructure and microchemistry. The Al–Si eutectic microstructure can be modified from coarse-faceted silicon particles nucleating at low undercooling to clusters of fine-scale silicon particles nucleating at high undercooling by either increasing alloy purity, adding sodium, or increasing cooling rate during solidification. The unmodified coarse silicon particles are heterogeneously nucleated on pre-existing AlP particles. Increasing alloy purity removes phosphorus and prevents the formation of AlP; adding sodium leads to the formation of Na_3P in preference to AlP; and increasing cooling rate allows insufficient time for the precipitation of AlP from low levels of dissolved phosphorus. At a cooling rate of $\sim 10\ K\,min^{-1}$, the transition from an unmodified to a modified Al–Si eutectic microstructure takes place when phosphorus levels fall below 0.25–2 p.p.m., and when sodium levels increase to 80–850 p.p.m.

1. Introduction

Al–Si alloys are commonly used in the foundry industry. However, the eutectic silicon in cast Al–Si alloys often exhibits a coarse microstructure which leads to poor mechanical properties. Pacz [1] discovered that eutectic silicon could be refined by melting Al–Si alloys under a flux of NaF, and a large number of papers have since attempted to explain this phenomenon, known as modification [2–10]. When Al–Si alloys are modified, the silicon microstructure undergoes a transition from coarse plates to a finer microstructure, often described as fibrous. A similar microstructural refinement can also be achieved by rapid quenching [9–12]. Accompanying the refinement of silicon microstructure is an increase in undercooling, as reported by Flood and Hunt [7], Hanna *et al.* [8] and Zhang and Cantor [13].

Nanometre-scale chemical analysis on a scanning transmission electron microscope (STEM) has shown that 99.995% pure Al–Si contains phosphorus- and aluminium-rich particles which are probably AlP and which nucleate silicon very efficiently at low undercooling to form coarse-faceted silicon particles [14]. Growth of the coarse-faceted silicon particles is thought to take place by silicon atoms attaching at twin plane re-entrant edges (TPRE) to form long thin particles, with the long axis parallel to the twin planes [6, 15, 17]. There is still considerable controversy as to how sodium modifies the silicon phase. One theory is that sodium affects the density of twins in the silicon phase either by poisoning TPRE sites [10] or by encouraging twinning [18] leading to more isotropic growth in all crystallographic directions. A second theory is that the plate to fibrous transition corresponds to an anisotropic faceted to isotropic non-faceted transition in silicon growth mode, and the effect of sodium is to alter the transition temperature [7]. A third theory is that sodium removes nucleating impurity particles such as AlP. Most investigations have concentrated on the growth theories of modification and relatively little work has been done on the nucleation theory.

The present study investigates nucleation effects in Al–Si alloys, using the entrained droplet technique devised by Wang and Smith [19], and recently modified by Moore *et al.* [20]. Melt spinning is used to manufacture a microstructure consisting of finely dispersed Al–Si eutectic droplets embedded in a higher melting point aluminium matrix. Extraneous impurity particles are segregated into an insignificant number of droplets. The alloys are then heated above the Al–Si eutectic temperature and cooled, so that the silicon phase is nucleated heterogeneously by the surrounding aluminium matrix. The solidification behaviour is studied using a differential scanning calorimeter (DSC), and the solidified microstructure is studied using a transmission electron microscope (TEM).

2. Experimental procedure

Al–Si, Al–Si–P, Al–Si–Na, and Al–Si–P–Na alloys were manufactured with different nominal purity as shown in Table I using Johnson Matthey 99.995% Al rods, 99.9999% Al shots, 99.9995% Si flakes, 99.7%

0022–2461

TABLE I Summary of elements found in 99.995% and 99.9999% Al–Si, Al–Si–P, Al–Si–Na and Al–Si–P–Na alloys

Alloy	Nominal Al purity (%)	P	Na	Mn	Fe
		(p.p.m.)			
Al–Si	99.995	2	–	< 1	3
Al–Si	99.9999	0.25	–	–	–
Al–Si–P	99.9999	35	–	–	–
Al–Si–Na	99.995	2	850	< 1	7
Al–Si–P–Na	99.999	0.5	80	50	50

AlP powder and 99.95% Na lumps. The aluminium was cleaned in NaOH solution and the other materials in methanol. The aluminium and silicon were then induction melted under argon, held above the liquidus temperature for 10 min to ensure a homogeneous melt, and cooled by switching off the furnace. For Al–Si–Na and Al–Si–P–Na, sodium and AlP were wrapped in aluminium foil to avoid evaporation and inserted into the Al–Si melt after holding for 10 min, using an alumina plunger to stir and ensure effective mixing. The resulting ingots were then ground on SiC paper to eliminate surfaces which had been in contact with the crucible wall and air, and cut into narrow strips ready for melt spinning.

For melt spinning, about 5 g ingot strips were remelted in argon in a quartz tube with an orifice at the bottom, held for 100 s, and then ejected with an argon overpressure of 20 kPa on to the surface of a copper wheel rotating at a speed of 20–25 $m\,s^{-1}$. The Al–Si–P alloy was manufactured by dipping the Al–Si ingot strips into AlP powder and ejecting the melt immediately on to the rotating copper wheel to avoid oxidation of the AlP powder.

The alloys all contained ~ 3 wt % Si. The levels of sodium and phosphorus as well as impurities such as manganese and iron were determined by emission spectroscopy at Johnson Matthey, and the results are given in Table I.

The silicon solidification behaviour in each melt-spun alloy was investigated by heat treatment in a TA2000 DSC by heating to 868 K, holding for 10 min, and cooling at a rate of 10 $K\,min^{-1}$ to 713 K. Alloy microstructures after heat treatment in the DSC were examined in a Philips CM20 TEM and VG HB501 STEM. Thin-foil specimens for electron microscopy were prepared by first grinding the heat-treated specimens on 1200 grade SiC paper until the specimens were about 60 μm thick, and then ion thinning with a gun voltage of 5 kV, a current of 0.5 mA and an angle of incidence of 15° in a Gatan duo ion thinner.

3. Results

3.1. General microstructures

The microstructure of all the heat-treated melt-spun alloys consisted of an aluminium matrix, Al–Si eutectic distributed along the grain boundaries and silicon distributed within the aluminium grains. The results of detailed TEM examination of silicon distributed within the aluminium grains are discussed in the following sections for each alloy in turn.

Figure 1 Bright-field TEM image of a twinned silicon particle in 99.995% Al–Si alloy.

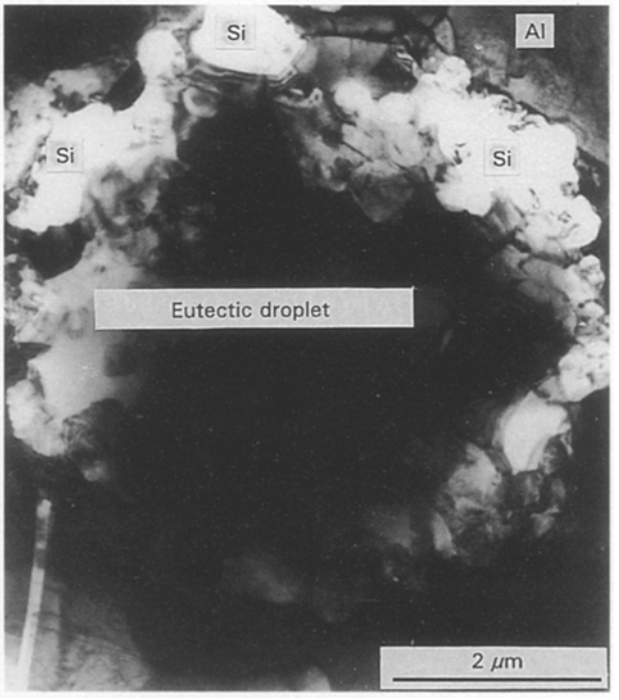

Figure 2 Bright-field TEM $[1\,1\,0]_{Al}$ image of a typical eutectic droplet in 99.9999% Al–Si alloy.

3.1.1. 99.995% Al–Si alloy microstructure

The microstructure of 99.995% Al–Si consisted of coarse-faceted silicon particles, a few micrometres in size and often twinned, embedded in the aluminium matrix. Fig. 1 shows a typical bright-field TEM image of one of the silicon particles containing an internal $\{1\,1\,1\}_{Si}$ twin boundary.

3.1.2. 99.9999% Al–Si alloy microstructure

The microstructure of 99.9999% Al–Si consisted of two-phase Al–Si eutectic droplets, 2–16 μm in size, embedded in the aluminium matrix. Fig. 2 shows a typical bright-field TEM image of one of the eutectic droplets. The eutectic droplets consisted of clusters of small silicon particles, 0.1–1 μm in size, together with aluminium. A shell of predominantly silicon particles

was present on the periphery of the eutectic droplets, as can be seen in Fig. 2.

3.1.3. Al–Si–P alloy microstructure

The microstructure of Al–Si–P, i.e. 99.9999% Al–Si with a small amount of AlP, was similar to 99.995% Al–Si rather than 99.9999% Al–Si, i.e. consisted of coarse-faceted silicon particles, a few micrometres in size and often twinned, embedded in the aluminium matrix. Fig. 3 shows a typical dark-field TEM image of one of the silicon particles using an Si g_{220} reflection.

3.1.4. Al–Si–Na alloy microstructure

The microstructure of Al–Si–Na, i.e. 99.995% Al–Si with a small amount of sodium, was similar to 99.9999% rather than 99.995% Al–Si, i.e. consisted of two-phase eutectic droplets, 2–16 μm in size, embedded in the aluminium matrix. The eutectic droplets consisted of clusters of small silicon particles, 0.1–1 μm in size, together with aluminium. Fig. 4 shows a bright-field TEM image of a typical eutectic droplet.

Fig. 5a–j shows a series of low- and high-magnification STEM X-ray elemental maps from another eutectic droplet. The silicon particle can be clearly seen in the bright silicon and complementary dark aluminium low-magnification STEM images in Fig. 5c and d. Within the silicon particle is a small region depleted in silicon and enriched in aluminium, as also shown in Fig. 5c and d. This region contained small amounts of oxygen and sodium, as shown in higher magnification STEM images in Fig. 5f and g. Fig. 5k shows an EDX spectrum from the same sodium-rich area within the silicon particle indicating the presence of oxygen, sodium, aluminium, silicon and phosphorus.

3.1.5. Al–Si–P–Na alloy microstructure

The microstructure of Al–Si–P–Na, i.e. 99.9999% Al–Si with small amounts of phosphorus and sodium, was similar to 99.995% Al–Si, and Al–Si–P, rather than 99.9999% Al–Si and Al–Si–Na, i.e. again consisted of coarse-faceted silicon particles, a few micrometres in size and often twinned, embedded in the aluminium matrix. Fig. 6 shows a typical bright-field TEM image from one of the silicon particles in Al–Si–P–Na, very similar to the silicon particles in 99.995% Al–Si and Al–Si–P as shown in Figs 1 and 3. The silicon particle in Fig. 6 shows small internal precipitates, labelled P.

Fig. 7a–n shows a series of low- and high-magnification STEM X-ray elemental maps from another silicon particle in Al–Si–P–Na. The silicon particle can be seen clearly in the bright silicon and dark aluminium low-magnification STEM images in Fig. 7c and d. Within the silicon particle is a small region depleted in silicon and enriched in aluminium as also shown in Fig. 7c and d. At low magnification, there was no sign of oxygen, sodium, phosphorus, manganese or iron within the region, as seen in Fig. 7a, b, e, f and g,

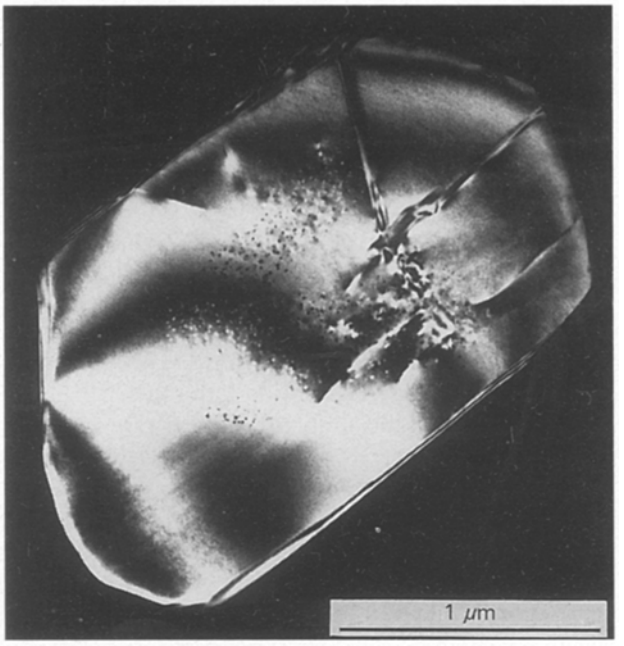

Figure 3 Dark-field TEM image of a silicon particle in Al–Si–P alloy using an Si g_{220} reflection.

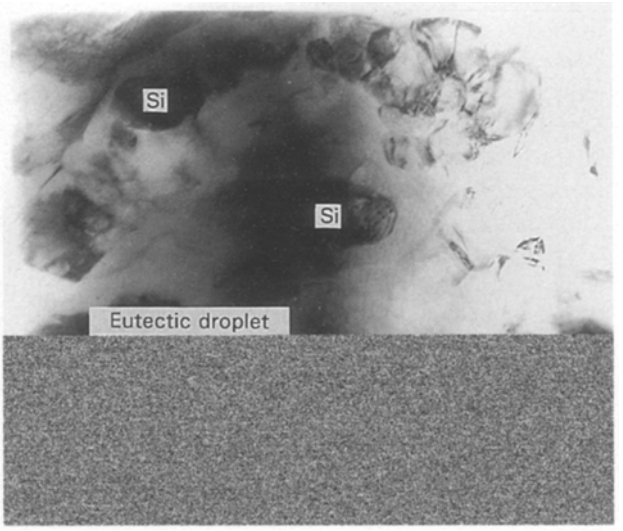

Figure 4 Bright-field TEM image of a typical eutectic droplet in Al–Si–Na alloy.

respectively. At higher magnification, however, a small phosphorus particle was found within the silicon-depleted and aluminium-enriched region, as seen in Fig. 7j, k and l. There was still no sign of oxygen, sodium, manganese or iron as seen in Fig. 7h, i, m and n, respectively. Fig. 7o shows an EDX spectrum from the same phosphorus-rich particle, indicating the presence of sodium, aluminium, silicon and phosphorus.

3.2. Nucleation of silicon solidification

Fig. 8a–e shows five sets of typical DSC traces of solidification exotherms obtained from 99.995% and 99.9999% Al–Si, Al–Si–P, Al–Si–Na and Al–Si–P–Na alloys, respectively, at a cooling rate of 10 K min^{-1}. The reproducibility of the DSC traces

as ± 2 K for all the alloys at this cooling rate. In all the alloys, two distinct solidification exotherms were seen. The first sharp exotherm, called A, always occurred at an onset temperature of about 847 K, i.e. 3 K below the equilibrium Al–Si eutectic temperature of 850 K. The second broader exotherm, called B, occurred at temperatures of $\sim$ 841, 790, 843, 802 and 843 K, i.e. 9, 60, 7, 48 and 7 K below the equilibrium Al–Si

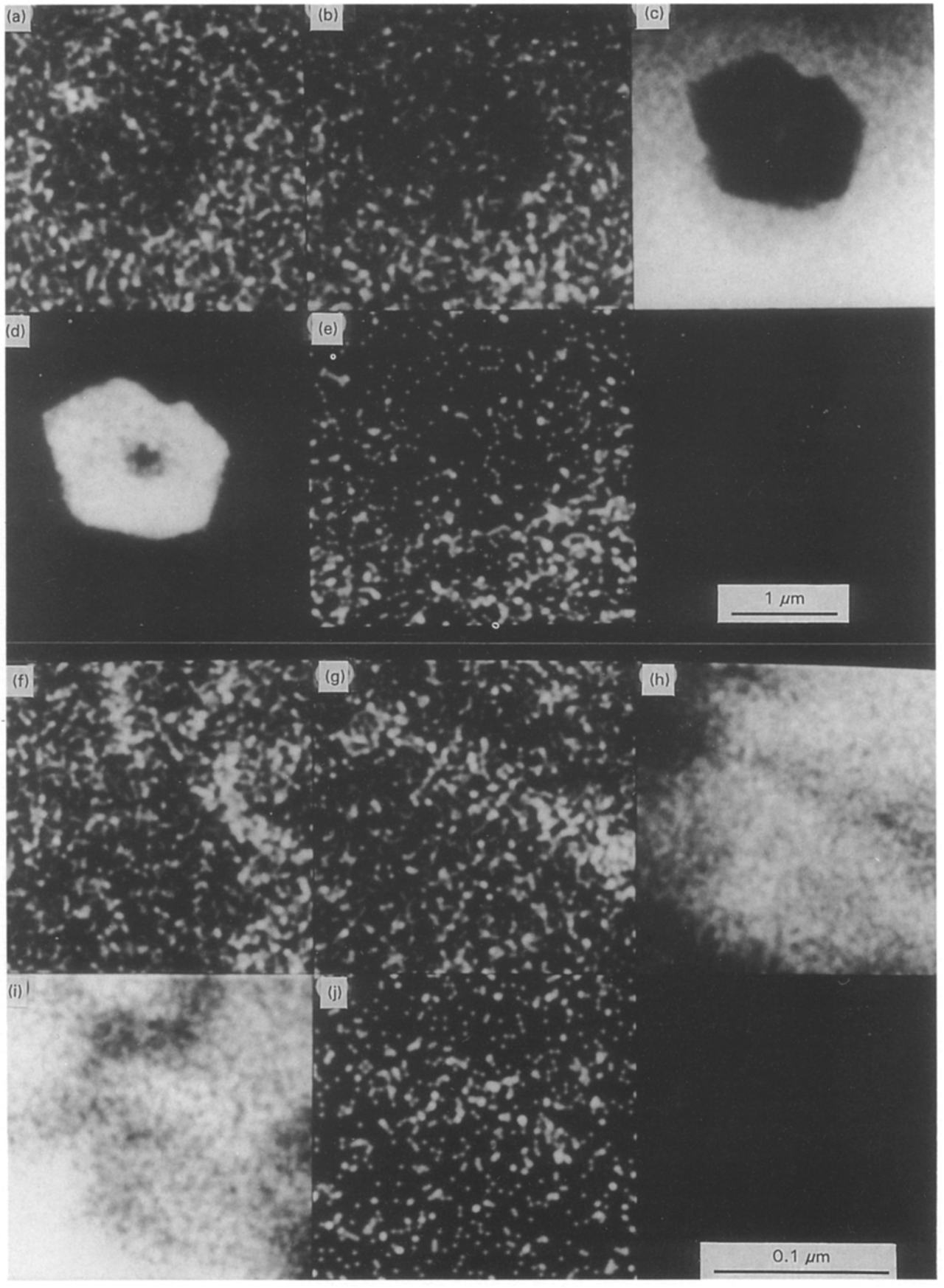

Figure 5 Low-magnification STEM X-ray elemental maps showing (a) oxygen, (b) sodium, (c) aluminium, (d) silicon and (e) phosphorus distribution in a silicon particle embedded in Al–Si–Na alloy; (f–j) are higher magnification images of (a–e) respectively; (k) EDX spectrum from the sodium-rich particle.

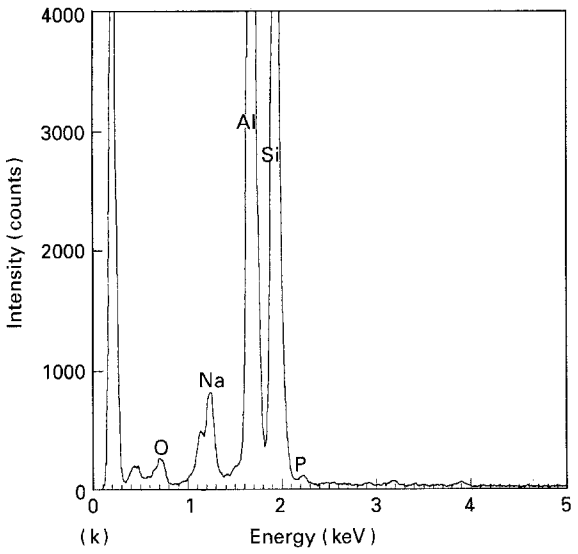

Figure 5 (continued)

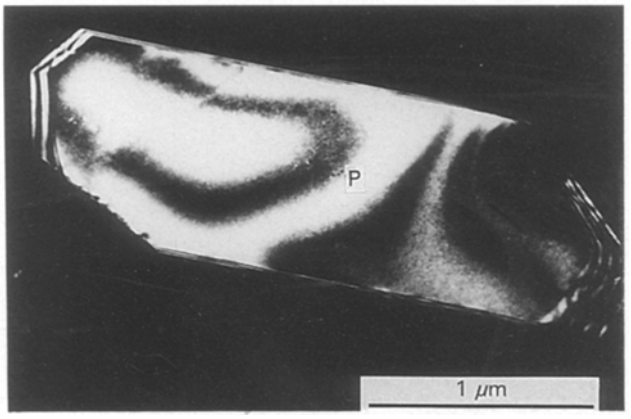

Figure 6 Dark-field TEM image of a silicon particle in the Al–Si–P–Na alloy using an Si g_{220} reflection.

eutectic temperature for the 99.995% and 99.9999% Al–Si, Al–Si–P, Al–Si–Na and Al–Si–P–Na alloys, as shown in Fig. 8a–e, respectively.

4. Discussion

4.1. Microstructures

The microstructures of the 99.9999% Al–Si and Al–Si–Na alloys consist of fine-scale Al–Si eutectic droplets as shown in Figs 2 and 4, i.e. refinement and modification of silicon takes place by increasing aluminium purity or by adding sodium. Full modification is achieved by reducing the phosphorus level below 2 p.p.m. or by adding 850 p.p.m. of sodium as shown in Table I. Unfortunately, it is difficult to determine the precise location of sodium in relation to the phosphorus in the Al–Si eutectic droplets. The microstructures of the 99.995% Al–Si, Al–Si–P and Al–Si–P–Na alloys consist of coarse-faceted silicon particles, as shown in Figs 1, 3 and 6. No refinement of silicon and no modification takes place when the phosphorus level is above 2 p.p.m. in 99.995% Al–Si and Al–Si–P, or when insufficient sodium (80 p.p.m.) is added in Al–Si–P–Na. Fig. 7l shows that a small phosphorus particle is located in the middle of a silicon particle in an aluminium-rich area. There is no sign of any other elements in this aluminium-rich area. However, EDX analysis on the phosphorus-rich area reveals the presence of a very small amount of sodium as seen in Fig. 7o. It seems conclusive from the EDX spectrum that the small phosphorus-rich particle contains sodium, aluminium and silicon.

4.2. Nucleation of silicon solidification

In all the alloys, two distinct solidification exotherms are seen, as shown in Fig. 8a–e. The first sharp exotherm always occurs at an onset temperature of about 847 K, i.e. 3 K below the equilibrium eutectic temperature of Al–Si. This sharp exotherm corresponds to solidification of grain-boundary eutectic, as shown previously by quenching experiments [21, 22]. The second, lower temperature, broader exotherm occurs at a different onset temperature depending on the alloy composition. The onset temperatures are 841, 790, 843, 802 and 843 K in 99.995% and 99.9999% Al–Si, Al–Si–P, Al–Si–Na and Al–Si–P–Na alloys, respectively. This peak corresponds to solidification of the Al–Si eutectic droplets distributed within the aluminium grains. Solidification of the eutectic Al–Si droplets takes place when fine-scale silicon particles are nucleated at high undercooling in the 99.9999% Al–Si and Al–Si–Na alloys, or when coarse-faceted silicon particles are nucleated at low undercooling in the 99.995% Al–Si, Al–Si–P and Al–Si–P–Na alloys. Modification of the silicon microstructure takes place when the silicon is nucleated at a high undercooling, and this is again achieved by either increasing aluminium purity to reduce phosphorus levels below 2 p.p.m., or by adding sufficient sodium.

4.3. Modification of Al–Si microstructure

4.3.1. Increasing aluminium purity

The microstructure of 99.9999% Al–Si consists of eutectic droplets of clusters of fine silicon particles randomly oriented with respect to the surrounding matrix, together with aluminium, all embedded in the surrounding aluminium matrix, as shown in Fig. 2. This indicates that the silicon microstructure is refined and that modification has been achieved without any ternary addition or rapid quenching. Modification can be explained on the basis that as the level of aluminium purity increases from 99.995% to 99.9999%, the phosphorus level decreases from 2 p.p.m. to 0.25 p.p.m., as shown in Table I. At this low level of phosphorus, there are insufficient AlP particles for effective heterogeneous nucleation of silicon from the eutectic Al–Si eutectic droplets. In the absence of AlP particles, the surrounding aluminium matrix heterogeneously nucleates silicon from eutectic Al–Si droplets at a higher undercooling, as shown in DSC traces in Fig. 8a and b. Aluminium is expected to be a relatively poor heterogeneous nucleant for silicon because of the dissimilar lattice parameters of 0.405 and 0.543 nm for aluminium and silicon, respectively.

4.3.2. Addition of sodium

The microstructure of 99.995% Al–Si with sodium added also consists of eutectic droplets of clusters of fine silicon particles together with aluminium, embedded in the surrounding aluminium matrix, as shown in Fig. 4. This indicates that the silicon microstructure is refined and that modification has been achieved by adding enough sodium to counteract the effect of phosphorus in impure 99.995% Al–Si. In contrast, modification is not achieved in the Al–Si–P–Na alloy, i.e. the microstructure still consists of coarse-faceted silicon particles, as shown in Fig. 6, similar to the

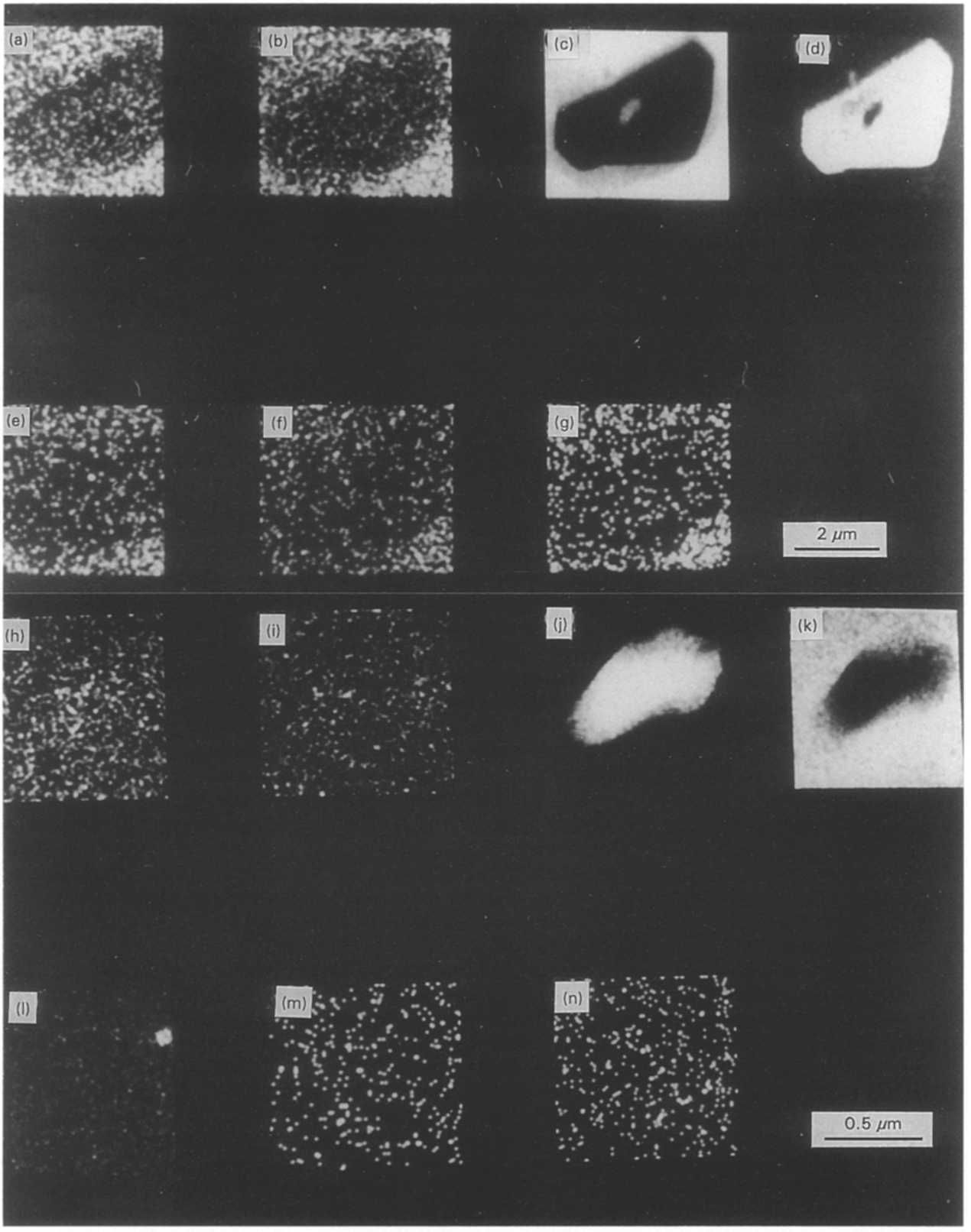

Figure 7 Low-magnification STEM X-ray elemental maps showing (a) oxygen, (b) sodium, (c) aluminium, (d) silicon, (e) phosphorus, (f) manganese and (g) iron distribution in a silicon particle embedded in an aluminium matrix in Al–Si–P–Na alloy; (h–n) are higher magnification images of (a–g), respectively; (o) EDX spectrum from the phosphorus-rich particle.

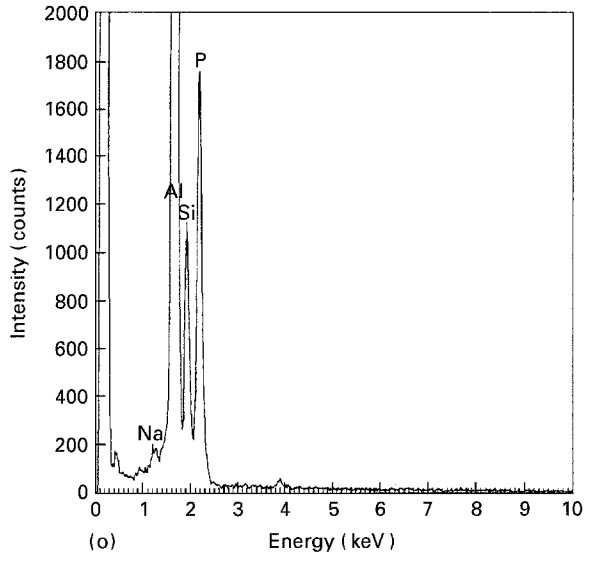

Figure 7 (continued)

99.995% Al–Si and the Al–Si–P alloy. The main growth theory of modification is that sodium affects the density of twins in the silicon phase, either by poisoning the TPRE sites, or by encouraging twinning, with the net result of a more isotropic growth in all crystallographic directions. However, many of the coarse-faceted silicon particles do not grow by the TPRE mechanism as the particles do not have the corresponding long thin shape, as shown in Fig. 1.

In comparison, relatively little work has been done on the alternative nucleation theory of modification that sodium removes the nucleation effect of impurity particles such as AlP [2, 3, 8]. It has been shown previously that AlP particles are present in 99.995% Al–Si and act as effective heterogeneous nucleants for silicon [14] and the present results indicate that modification takes place by sodium removing the nucleating AlP particles. STEM X-ray elemental maps, such as Fig. 5g, show that the sodium addition is localized in small particles, rather than being adsorbed uniformly in the aluminium or silicon phases and STEM EDX spectra such as Fig. 5k show that sodium is concentrated in phosphorus-rich regions of the Al–Si eutectic droplets. The effect of sodium is probably to form Na_3P in preference to AlP. In the absence of AlP, the surrounding aluminium matrix nucleates silicon inefficiently at relatively high undercooling, as shown

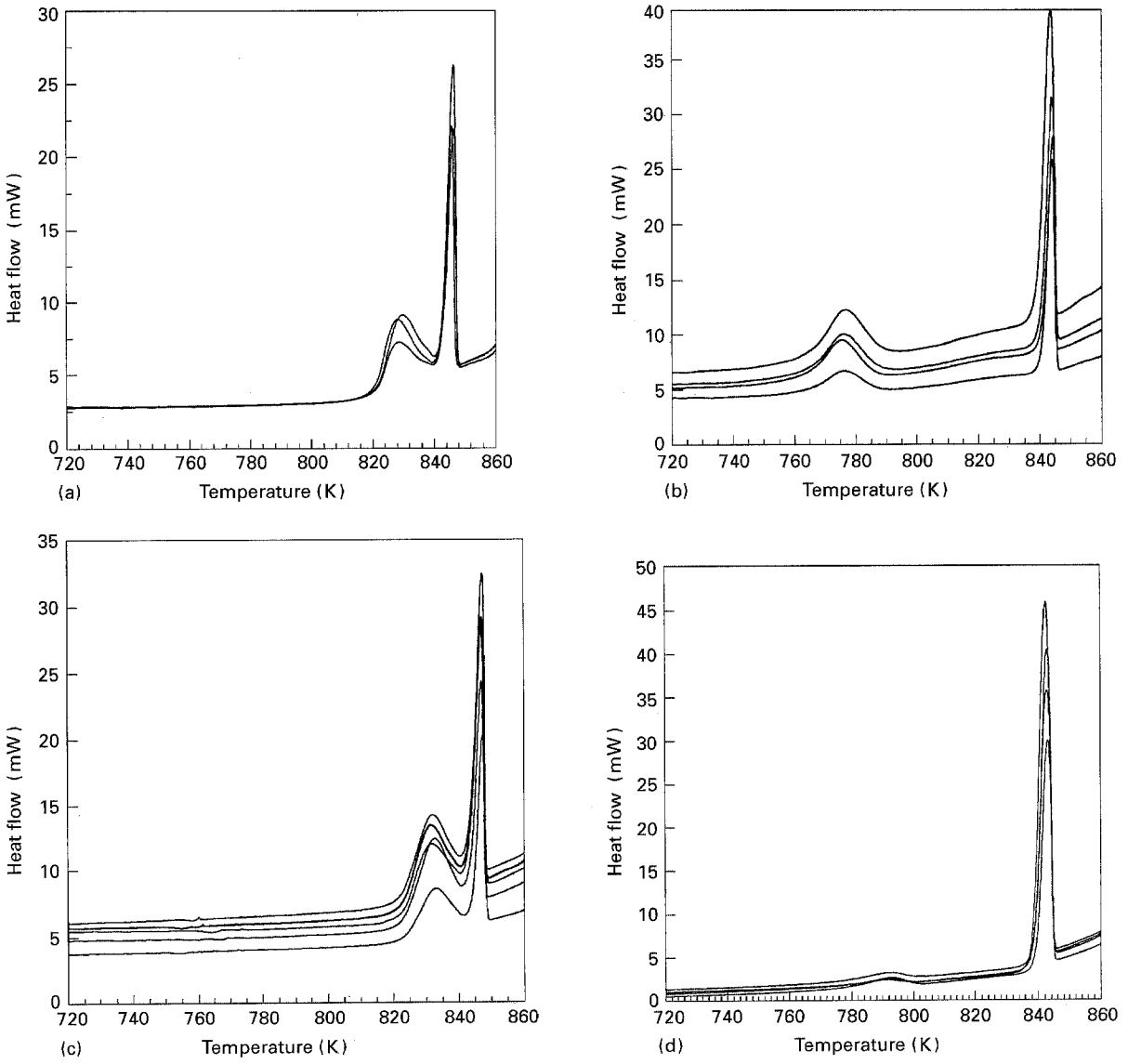

Figure 8 DSC traces of solidification exotherms in (a) 99.995% Al–Si, (b) 99.9999% Al–Si, (c) Al–Si–P, (d) Al–Si–Na and (e) Al–Si–P–Na alloys at a cooling rate of 10 K min^{-1}.

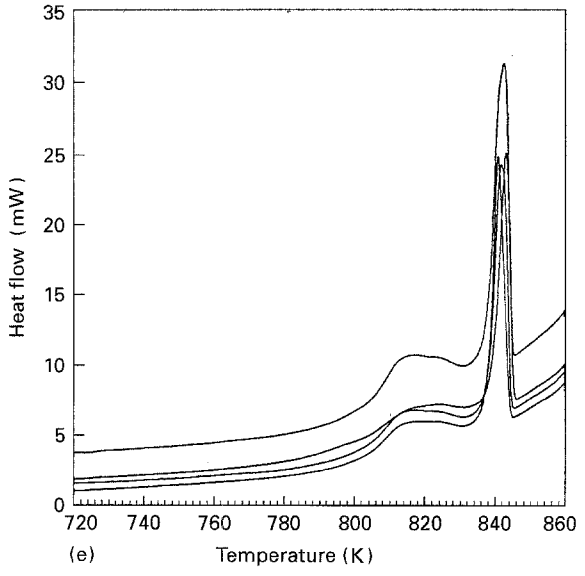

Figure 8 (continued)

in the DSC traces such as Fig. 8, to give the modified microstructure of clusters of fine-scale silicon particles.

It is well-established foundry practice that ~ 0.01 wt % Na, i.e. 100 p.p.m. is required to produce full modification [7, 8]. This is in agreement with the present results with 850 p.p.m. Na producing modification in Al–Si–Na, but 80 p.p.m. Na is insufficient in Al–Si–P–Na, as shown in Figs 4 and 6 and Table I. Clapham and Smith [23] have suggested that the sodium concentration required to produce modification depends on its solubility in the primary aluminium phase. This proposal was based on their findings that modifiers segregate preferentially to and are absorbed in the silicon phase, and this was explained by the fact that during solidification the modifier was rejected by the aluminium phase, being more or less insoluble in aluminium.

The concentration of sodium required to form Na_3P instead of AlP is given by $c_{Na} = 3x(w_{Na}/w_p)c_p$ where w_{Na} and w_p are the atomic weights of sodium and phosphorus respectively, and c_p is the impurity phosphorus concentration. Substituting 22.99 and 30.97 g for w_{Na} and w_p, respectively [24], gives $c_{Na} \approx 2c_p$ to form Na_3P. Thus only 4 p.p.m. Na should be needed in 99.995% Al–Si with $c_p = 2$ p.p.m., only 1 p.p.m. Na should be needed in Al–Si–P–Na with $c_p = 0.5$ p.p.m. and only 20 p.p.m. Na should be needed in foundry alloys with phosphorus levels up to 10 p.p.m. However, 80 p.p.m. Na is insufficient to produce full modification in Al–Si–P–Na even though there is enough sodium to react fully with all the phosphorus, as shown in Table I. On the other hand, 850 p.p.m. Na is sufficient to react with all the phosphorus and produce full modification in Al–Si–Na, but it is unclear why so much sodium is needed. This implies that the mechanism of modification is not simply the formation of Na_3P instead of AlP. Exceeding the sodium solubility in aluminium or silicon before forming Na_3P might explain why more than 80 p.p.m. Na is needed for full modification.

4.3.3. Rapid quenching

Zhang and Cantor [13] have shown that when 99.995% Al–Si is quenched from 868 K, i.e. above the equilibrium Al–Si eutectic temperature of 850 K, the silicon microstructure is similar to 99.9999% Al–Si and Al–Si–Na, i.e. eutectic droplets consisting of fine silicon particles randomly oriented with respect to the aluminium matrix. In other words, modification can be achieved in 99.995% Al–Si by rapid quenching. The coarse-faceted silicon particles are nucleated by AlP particles formed from phosphorus and aluminium [14]. However, rapid quenching gives insufficient time for recombination of phosphorus and aluminium, so that AlP nucleant particles are not formed. In the absence of AlP particles, the surrounding aluminium matrix heterogeneously nucleates silicon from the Al–Si eutectic droplets at a high undercooling to produce the microstructure of clusters of fine silicon particles in Al–Si eutectic droplets.

5. Conclusions

Entrained droplet studies of hypoeutectic Al–Si–P–Na alloys show that the Al–Si eutectic microstructure can be modified from coarse-faceted silicon particles nucleating at low undercooling to clusters of fine-scale silicon particles nucleating at high undercooling by either increasing alloy purity, adding sodium, or increasing cooling rate during solidification. The unmodified coarse silicon particles are heterogeneously nucleated on pre-existing AlP particles. Increasing alloy purity removes phosphorus and prevents the formation of AlP; adding sodium leads to the formation of Na_3P in preference to AlP; and increasing cooling rate allows insufficient time for the precipitation of AlP from low levels of dissolved phosphorus. At a cooling rate of $\sim 10\,K\,min^{-1}$, the transition from an unmodified to a modified Al–Si eutectic microstructure takes place when phosphorus levels fall below 0.25–2 p.p.m., and when sodium levels increase to 80–850 p.p.m.

Acknowledgements

We thank Dr N. J. Long for help with the STEM, and SERC and Foseco International for financial support.

References

1. A. PACZ, US Pat. 1387900 (1921), Br. Pat. 158 827.
2. R. C. PLUMB and J. E. LEWIS, *J. Inst. Metals* **86** (1957) 393.
3. V. DE L. DAVIES and T. M. WEST, *ibid.* **92** (1963) 175.
4. C. B. KIM and P. W. HEINE, *ibid.* **92** (1963) 367.
5. H. FREDRIKSSON, M. HILLERT and N. LANGE, *ibid.* **101** (1973) 285.
6. H. A. H. STEEN and A. HELLAWELL, *Acta Metall.* **23** (1975) 529.
7. S. FLOOD and J. D. HUNT, *Metall. Sci.* **15** (1981) 287.
8. M. D. HANNA, S. Z. LU and A. HELLAWELL, *Metall. Trans.* **15A** (1984) 459.
9. S. Z. LU and A. HELLAWELL, *J. Crystal Growth* **73** (1985) 316.
10. K. F. KOBAYASHI and L. M. HOGAN, *J. Mater. Sci.* **20** (1985) 1961.

11. H. A. H. STEEN and A. HELLAWELL, *Acta Metall.* **20** (1972) 363.
12. M. SHAMSUZZOHA and L. M. HOGAN, *J. Crystal Growth* **82** (1987) 598.
13. D. L. ZHANG and B. CANTOR, *Metall. Trans.* **24A** (1993) 1195.
14. C. R. HO and B. CANTOR, University of Oxford, Oxford, UK, unpublished research (1994).
15. K. KOBAYASHI, P. H. SHINGU and R. OZAKI, in "International Conference on Solidification and Casting of Metals", edited by I. G. Davies and R. Jordan (Metals Society, London, 1979) p. 101.
16. M. SHAMSUZZOHA and L. M. HOGAN, *J. Crystal Growth* **76** (1986) 429.
17. *Idem, Metallography* **22** (1989) 37.
18. M. G. DAY and A. HELLAWELL, *Proc. R. Soc.* **A305** (1968) 473.
19. G. C. WANG and C. S. SMITH, *Trans. AIME* **188** (1950) 136.
20. K. I. MOORE, D. L. ZHANG and B. CANTOR, *Acta Metall.* **38** (1990) 1327.
21. R. T. SOUTHIN, PhD thesis, University of Cambridge (1970).
22. D. L. ZHANG, DPhil thesis, University of Oxford (1990).
23. L. CLAPHAM and R. W. SMITH, in "Solidification Processing" (Sheffield, 1987).
24. E. A. BRANDES and G. B. BROOK (eds), "Smithells Metals Reference Book", 7th Edn (Butterworth Heinemann, Oxford).

Received 16 August
and accepted 10 October 1994